Cell Transplantation, Vol. 21, pp. 2225–2239, 2012

0963-6897/12 $90.00 + .00
DOI: http://dx.doi.org/10.3727/096368912X653020
E-ISSN 1555-3892
www.cognizantcommunication.com

Improved Cell Survival and Paracrine Capacity of Human Embryonic Stem Cell-Derived Mesenchymal Stem Cells Promote Therapeutic Potential for Pulmonary Arterial Hypertension

Yuelin Zhang,* Songyan Liao,* Mo Yang,†‡ Xiaoting Liang,* Ming-Wai Poon,* Chee-Yin Wong,§ Junwen Wang,¶ Zhongjun Zhou,¶ Soon-Keng Cheong,§ Chuen-Neng Lee,# Hung-Fat Tse,*,** and Qizhou Lian*,**††

*Cardiology Division, Department of Medicine, University of Hong Kong, Hong Kong
†Department of Hematology, Nanfang Hospital, Southern Medical University, Guangzhou, PR China
‡Department of Pharmacology and Pharmacy, Li Ka Shing Faculty of Medicine, University of Hong Kong, Hong Kong
§MAKNA Cancer Research Institute, Kuala Lumpur, Malaysia
¶Department of Biochemistry, University of Hong Kong, Hong Kong
#Department of Surgery, National University Hospital, National University of Singapore, Singapore
**Research Centre of Heart, Brain, Hormone, and Healthy Aging, Li Ka Shing Faculty of Medicine, University of Hong Kong, Hong Kong
††Eye Institute, Li Ka Shing Faculty of Medicine, University of Hong Kong, Hong Kong

Although transplantation of adult bone marrow mesenchymal stem cells (BM-MSCs) holds promise in the treatment for pulmonary arterial hypertension (PAH), the poor survival and differentiation potential of adult BM-MSCs have limited their therapeutic efficiency. Here, we compared the therapeutic efficacy of human embryonic stem cell-derived MSCs (hESC-MSCs) with adult BM-MSCs for the treatment of PAH in an animal model. One week following monocrotaline (MCT)-induced PAH, mice were randomly assigned to receive phosphate-buffered saline (MCT group); 3.0×10^6 human BM-derived MSCs (BM-MSCs group) or 3.0×10^6 hESC-derived MSCs (hESC-MSCs group) via tail vein injection. At 3 weeks posttransplantation, the right ventricular systolic pressure (RVSP), degree of RV hypertrophy, and medial wall thickening of pulmonary arteries were lower=, and pulmonary capillary density was higher in the hESC-MSC group as compared with BM-MSC and MCT groups (all $p<0.05$). At 1 week posttransplantation, the number of engrafted MSCs in the lungs was found significantly higher in the hESC-MSC group than in the BM-MSC group (all $p<0.01$). At 3 weeks posttransplantation, implanted BM-MSCs were undetectable whereas hESC-MSCs were not only engrafted in injured pulmonary arteries but had also undergone endothelial differentiation. In addition, protein profiling of hESC-MSC- and BM-MSC-conditioned medium revealed a differential paracrine capacity. Classification of these factors into bioprocesses revealed that secreted factors from hESC-MSCs were preferentially involved in early embryonic development and tissue differentiation, especially blood vessel morphogenesis. We concluded that improved cell survival and paracrine capacity of hESC-MSCs provide better therapeutic efficacy than BM-MSCs in the treatment for PAH.

Key words: Pulmonary arterial hypertension; Embryonic stem cell-derived mesenchymal stem cells

INTRODUCTION

Pulmonary arterial hypertension (PAH) is a life-threatening disease characterized by increased arterial medial thickness, intimal fibrosis, and arteriolar occlusion of the pulmonary circulation. These pathological changes result in progressive elevation of pulmonary arterial pressure, right ventricular (RV) failure, and death (26). Despite recent advances in pharmacological therapy, including the use of an endothelin receptor antagonist and phosphodiesterase type 5 inhibitor, the only cure for this devastating disease is lung transplantation (4). This is nonetheless limited by a shortage of available donor organs and the risk of lung graft rejection (19). Recent experimental and clinical studies suggest that transplantation of bone marrow (BM)-derived mesenchymal stem cells (MSCs) (3,15,16,24) may attenuate the progression of PAH and restore lung and

Received October 7, 2010; final acceptance October 10, 2011. Online prepub date: July 5, 2012.
Address correspondence to Qizhou Lian, M.D., Ph.D., *or* Hung-Fat Tse, M.D., Ph.D., Cardiology Division, Department of Medicine, Queen Mary Hospital, The University of Hong Kong, Hong Kong. Tel: +852-21899752; Fax: +852-28162095;
E-mail: qzlian@hkucc.hku.hk (Qizhou Lian), hftse@hkucc.hku.hk (Hung-Fat Tse)

heart function. However, there are several potential limitations of using BM-MSCs. Firstly, BM-MSCs display a limited proliferative capacity and a large variability of cell quality derived from different donors. Secondly, during ex vivo expansion before possible therapeutic use, these cells quickly lose differentiation potential and the ability to produce protective factors (7,43). Importantly, survival capacity and stem cell functions of BM-MSCs derived from aged or diseased donors (i.e., PAH) are profoundly impaired (15) and thus limit their therapeutic efficacy (12,34,44). Therefore, it is desirable to identify more therapeutically useful stem cells for more effective treatment of PAH.

Recently, we have derived functional MSC lines from human pluripotent stem cells (21,23). Compared with adult BM-derived MSCs, pluripotent stem cells-derived MSCs have a higher potential for proliferation and differentiation. For instance, human embryonic stem cell-derived MSCs (hESC-MSCs) can be expanded in more than 25 passages without obvious senescence and also demonstrate an ability to differentiate into multiple cell types. On the other hand, adult BM-MSCs quickly become senescent after a short-term expansion (21). Similar to hESC-MSCs, human-induced pluripotent stem cell-derived MSCs (23) may also be an invaluable cell source in the treatment of PAH and overcome many disadvantages of using BM-MSCs. Nevertheless, the therapeutic efficacy of pluripotent stem cells-derived MSCs in PAH has not been determined yet. In this study, we demonstrated that pluripotent hESC-derived MSCs are superior to adult BM-derived MSCs in the attenuation of PAH induced by monocrotaline (MCT) injection. Compared with BM-MSCs, the greater therapeutic potential of hESC-MSCs might be attributed to their ability to survive longer after transplantation as well as the more robust capacity to promote pulmonary arterial regeneration via direct de novo vascular differentiation or/and great paracrine mechanisms.

MATERIALS AND METHODS

Generation and Characterization of Human ES Cell Line-Derived Mesenchymal Stem Cells

Clinically compliant MSCs derived from hESC lines have been described previously (21). In this study, MSCs derived from the HES-3 cell line (WiCell® Research Institute) were used as hES-3 cells have a great potential for cardiovascular differentiation (30). Briefly, a confluent 6-cm plate of hES3 cells was trypsinized on a gelatinized 10-cm dish containing enrichment of MSC outgrowth medium: Dulbecco's modified Eagle's medium (DMEM) (Gibco, Grand Island, NY) supplemented with 10% serum replacement medium (Gibco), 10 ng/ml basic fibroblast growth factor (bFGF; Gibco), 10 ng/ml dimeric platelet-derived growth factor A and B chain (PDGFAB), and 10 ng/ml epidermal growth factor (EGF; Peprotech, Rocky Hill, NJ). One week after hES3 cells under above differentiation medium, the differentiating hES3 cells were harvested and sorted for $CD24^{-}CD105^{+}$ subpopulation. The $CD24^{-}CD105^{+}$ cells were seeded in a 10-cm cultural dish with limiting dilution (1,000 cells/per 10-cm dish) and allow single cell-derived colonies to grow up. When colonies were formed and grown up, each clone was picked up and transferred to a six-well plate that was serially reseeded thereafter in 25 cm^2 and 75 cm^2. A total of four clone lines were achieved in this manner. Clones of hES3-MSC2 were selected for continuous cultures. MSCs derived from the hES-3 cell line (hESC-MSCs) were characterized by surface antigen profiling, adipogenesis, osteogenesis, and chondrogenesis studies (21). Oil red staining for adipocytes, Alizarin Red staining for osteocytes, and Alcian Blue staining for chondrocytes were used as standard techniques. Characterized human adult BM-MSCs were commercially acquired from Cambrex BioScience (Cat. No. PT-2501). All human materials used in this study were approved by the ethical committee of the University of Hong Kong.

Animal Model of PAH

PAH was induced in adult mice (ICR strain, provided by the laboratory animal unit of the University of Hong Kong) by intraperitoneal injection of MCT (6). In the negative control group, mice were injected with saline ($n=15$). To establish the animal model of PAH and minimize nonspecific acute lung injuries induced by overdose of MCT injection, three dosages of MCT (200, 400, and 600 mg/kg) were tested in a pilot study. We observed no evidence of PAH in 200 mg/kg-treated group ($n=10$) but a high mortality (70%) in 600 mg/kg-treated group ($n=10$). As a result, we choose the dosage of 400 mg/kg in our experiment as previously reported (34) and confirmed the successful creation of an animal model of PAH by measuring RV systolic pressure (RVSP) at 1 week following MCT administration ($n=15$). A further group of animals were randomized to receive intravenous administration of (1) phosphate-buffered saline (PBS, MCT group, $n=15$), (2) 3.0×10^6 BM-MSCs (BM-MSCs group, $n=15$), or (3) 3.0×10^6 hESC-MSCs (hESC-MSC group, $n=15$) via tail vein injection 1 week following administration of MCT. A subgroup of mice in each group ($n=6$) were sacrificed 1 week following transplantation to determine cell retention and survival. The remaining animals ($n=9$ each group) were kept for 3 weeks following transplantation when final hemodynamic assessment was made. All animals were treated with 15 mg/kg/day cyclosporine for 2 days before and daily after transplantation. In addition, 3.0×10^6 BM-MSCs were also injected into three severe combined immunodeficient (SCID, provided by the laboratory animal unit of the University of Hong Kong) mice via tail vein injection. After 3 weeks of cell injection,

SCID mice were sacrificed for histological examination. All experiments were approved by the Committee on the Use of Live Animals in Teaching and Research (CULTAR) at the University of Hong Kong.

Hemodynamic Assessment

At 3 weeks posttransplantation, mice were anesthetized (induction with intraperitoneal injection of 100 mg/kg of ketamine and 20 mg/kg of xylazine) and mechanically ventilated. Blood pressure was measured by the tail-cuff method using a noninvasive automatic blood pressure recorder (Visitech System BP-2000 Blood Pressure Analysis System, USA). Average values of arterial systolic BP (SBP) were derived from three consecutive measurements. A 1.4-Fr high-fidelity microtip catheter connected to a pressure transducer (Millar Instruments, Houston, TX, USA) was inserted into the RV cavity via the right internal jugular vein to record RVSP using the PowerLab system (AD Instruments, Inc., Colorado Springs, CO, USA).

Assessment of RV Hypertrophy

Mice were sacrificed following hemodynamic assessment for histological and immunohistochemical examination. After removal of the heart, the RV free wall was excised from the left ventricular (LV) wall and the interventricular septum. The ratio of the weight of the RV to LV plus septum [RV/(LV + septum)] was calculated as an index of RV hypertrophy (18).

Polymerase Chain Reaction (PCR)

Genomic PCR for human *Alu-sx* repeat sequences and mouse *c-mos* repeat sequences were performed as previously described (21). Telomerase activity was performed by Telomeric Repeat Amplification Protocol (TRAP) as described previously (21,23) and according to manufacturer's recommendations (Allied Biotech, Cat. No. MT 3010). Each sample was analyzed at least in duplicates. Telomerase activity was expressed relative to BM-MSCs. Reverse transcription (RT)-PCR for human-specific fibroblast growth factor 2 (FGF2), von Willebrand factor (vWF), vascular endothelial growth factor (VEGF), and vascular endothelial growth factor receptor 2 (Flk-1) was performed in a total volume of 20 ml with 20 nmol of each primer. The primers were as follows: hvWF: F5′-TGACGGTGAATGGGAGACTGG-3′, R5′-GCATGAAGTCATTGGCTCCGTTC-3′; hVEGF: F5′-GCAGAAGGAGGAGGGCAGAATC-3′, R5′-CACT CCAGGCCCTCGTCATT-3′; hFGF2: F5′-GAAGA GCGACCCTCACATCAAG-3′, R5′-CTGCCCAGTTCGT TTCAGTG-3′; GADPH: F5′-GTCTTCACCACCATG GAGAAGG-3′, R5′-GCCTGCTTCACCACCTTCT TGA-3′; VEGFR2 (also named Flk-1): F5′-GTGACCAA CATGGAGTCGTG -3′, R5′-CCAGAGATTCCATG CCACTT-3′.

Histological Analysis, Immunohistochemical Staining, and Cytokine Assays

The lungs were fixed with 10% buffered formalin and embedded in paraffin, then sectioned to 5-μm slides, and stained with hematoxylin and eosin. Morphometric analysis was performed on pulmonary muscular arteries whose external diameter ranged from 25 to 100 μm, using a color digital camera mounted on a computer-interfaced light microscope. Medial wall thickness was measured as the distance between the external and internal elastic lamina of each artery using a calibrated eyepiece micrometer; external diameter was measured as the diameter of the external lamina. The percentage medial wall thickness of each artery was calculated using the following: % medial wall thickness = 2 × medial wall thickness/external diameter × 100. For each lung section, 20 pulmonary arteries were measured, and the average value calculated (29).

Standard procedures were applied for immunohistochemical staining (22). The lung sections were prepared with a cryostat and immunostained with goat anti-CD31 (Santa Cruz, SC-1506), human nuclear antigen (HNA) polyclonal antibody (MAB1281, Chemicon). The primary antibodies were incubated overnight at 4°C with a 1:100 dilution. Then secondary antibodies with a 1:200 dilution were used against the primary antibodies. For fluorescent immunostaining, sections were analyzed using a deconvoluted fluorescent microscope and Metamorph software.

For simultaneous detection of BM-MSC- and hESC-MSC-derived paracrine factors, serum-free cell culture supernatants of BM-MSCs and hESC-MSCs were harvested, filtered through a 0.22-μm filter, and concentrated (38). A total of 200 μl of conditioned or nonconditioned medium was assayed for the presence of cytokines and other proteins using RayBio® Cytokine Antibody Arrays according to the manufacturer's instructions (RayBiotech, Norcross, GA, Cat. No. AAH-BLG-1-4). Quantitative human cytokines were measured using customized Bio-Plex cytokine assays (Bio-Rad Laboratories, Hercules, CA, Cat. Nos. M50007VNJK and MF00038C9E) according to the manufacturer's instructions.

Statistical Analysis

Data are expressed as mean ± standard derivation. Statistical analysis was performed with ANOVA followed by the Bonferroni test for multiple comparisons between different study groups. A value of $p < 0.05$ was considered statistically significant.

RESULTS

Characterization of hES-3-Derived MSCs

Unlike its parental hES-3 cell line, the hES-3 cell line-derived MSCs (hESC-MSC) were highly similar to adult BM-MSCs in morphology (Fig. 1A, i). Adipogenesis was highly efficient with oil red droplets observed in >80%

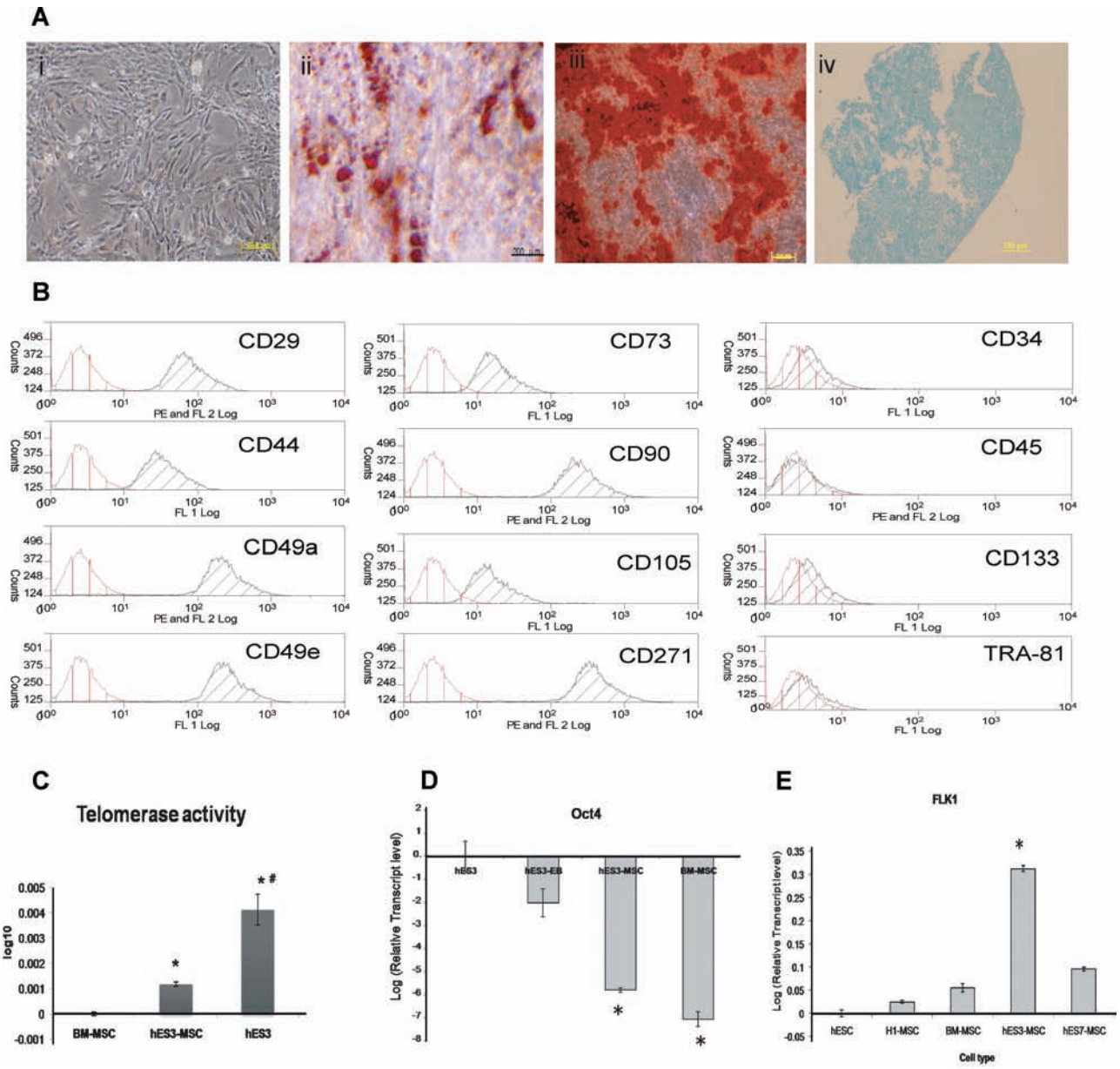

Figure 1. (A) The typical morphology of human embryonic stem cell line hES-3-derived mesenchymal stem cells (MSCs) (hESC-MSCs). (i) Scale bar: 20 μm. Oil Red staining for adipogenesis. (ii) Scale bar: 200 μm. Alizarin Red staining for osteogenesis. (iii) Scale bar: 200 μm. Alcian Blue staining for chondrogenesis. (iv) Scale bar: 200 μm. (B) Surface markers profiling by fluorescence activated cell sorting (FACS) in hES3-MSC cultures for CD29, CD44, CD49a, CD49e, CD73, CD90, CD105, CD271, CD34, CD45, CD133, and TRA-81. (C) Differential telomerase activity among bone marrow (BM)-MSCs, hESC-MSCs, and hES-3 (*$p<0.001$ vs. BM-MSCs; #$p<0.001$ vs. hESC-MSC). (D) Transcript levels of pluripotency-associated gene Oct4 were measured by quantitative reverse transcription-polymerase chain reaction (PCR) and normalized to that of hES-3 (*$p<0.01$ vs. hES-3). (E) Following exposure of cells to endothelial differentiation medium for 3 days, transcript levels of endothelial differentiation marker Flk-1 were measured among hESCs, hESC-MSCs, and BM-MSCs by quantitative reverse transcription-polymerase chain reaction (qRT-PCR) and normalized to that of hES-3 (*$p<0.001$ vs. BM-MSCs).

of the hESC-MSCs (Fig. 1A, ii). Osteogenesis was efficient with >80% cells had Alizarin Red staining for calcium deposition (Fig. 1A, iii). Chondrogenesis was also efficient with >90% of cells producing proteoglycans in extracellular matrix as detected by Alcian Blue staining (Fig. 1A, iv). These hESC-MSCs also expressed similar surface antigen profiling, which defined BM-MSCs, that is, CD29$^+$, CD44$^+$, CD49a and e$^+$, CD73, CD90$^+$, CD105$^+$, CD271$^+$ and CD34$^-$, CD45$^-$, CD133$^-$ as demonstrated by fluorescence-activated cell sorting (FACS) analysis (Fig. 1B). These hESC-MSCs were not contaminated with undifferentiated hESCs as they are negative for hESC

surface marker TRA-81 (Fig. 1B). Furthermore, hESC-MSCs were highly expandable up to 30 passages (90 population doublings) without obvious loss of self-renewal capacity and constitutively express surface antigens of multipotent MSCs.

To understand the molecular basis of the high proliferation potential of hESC-MSCs, telomerase activity was compared among BM-MSCs, hESC-MSCs, and hESCs. It revealed more than 10-fold higher level of telomerase activity in hESC-MSCs (passage 25) than in BM-MSCs (passage 5) (Fig. 1C). This might account for the greater capacity of cell proliferation in hESC-MSCs than BM-MSCs. Above passage 40, random chromosomal aberrations were observed by karyotyping. Therefore, these hESC-MSCs were chromosomally stable up to at least passage 40 (120 population doublings), and thus, hESC-MSCs below passage 30 were used for this study.

Expression of pluripotency-associated genes was generally reduced in hESC-MSCs. For example, expression of pluripotent gene Oct4 was significantly reduced 10,000 times compared to hES-3 cells (Fig. 1D). To confirm the loss of pluripotency in hESC-MSCs, 1×10^6 hESC-MSCs were subcutaneously transplanted into SCID mice. The transplanted hESC-MSCs did not appear to survive or engraft into the normal recipient tissue (data not show). The endothelial differentiation potential of BM-MSCs, hESC-MSCs, and hESCs was compared by measuring the expression level of human VEGFR2 (also named Flk-1) with qRT-PCR. As shown in Figure 1E, the expression level of Flk-1 in hESC-MSCs was significantly higher than those in BM-MSCs or hESCs.

Hemodynamic Changes of PAH and MSC Transplantation

The experimental protocol was shown in Figure 2A. To determine the effects of MCT administration on pulmonary and systemic circulation, the RVSP and SBP of mice were measured. Compared with the control group (27.4 ± 0.70 mmHg), RVSP was significantly increased at 1 week (40.24 ± 3.32 mmHg, $p < 0.05$) and 4 weeks (59.12 ± 4.32 mmHg, $p < 0.01$) following MCT administration. This confirmed successful induction of PAH by MCT administration (Fig. 2B). Similarly, the degree of relative pulmonary hypertension measured by the ratio of RVSP/SBP was also significantly increased at 4 weeks in the MCT group as compared with control (Fig. 2C) ($p < 0.01$). However, there were no difference in SBP between the control and study mice at 4 weeks following MCT administration (Fig. 2D) ($p > 0.10$), suggesting that MCT-induced vascular injuries mainly limited in pulmonary circulation.

Since elevated RVSP was evident at 1 week following MCT administration, we decided to examine the

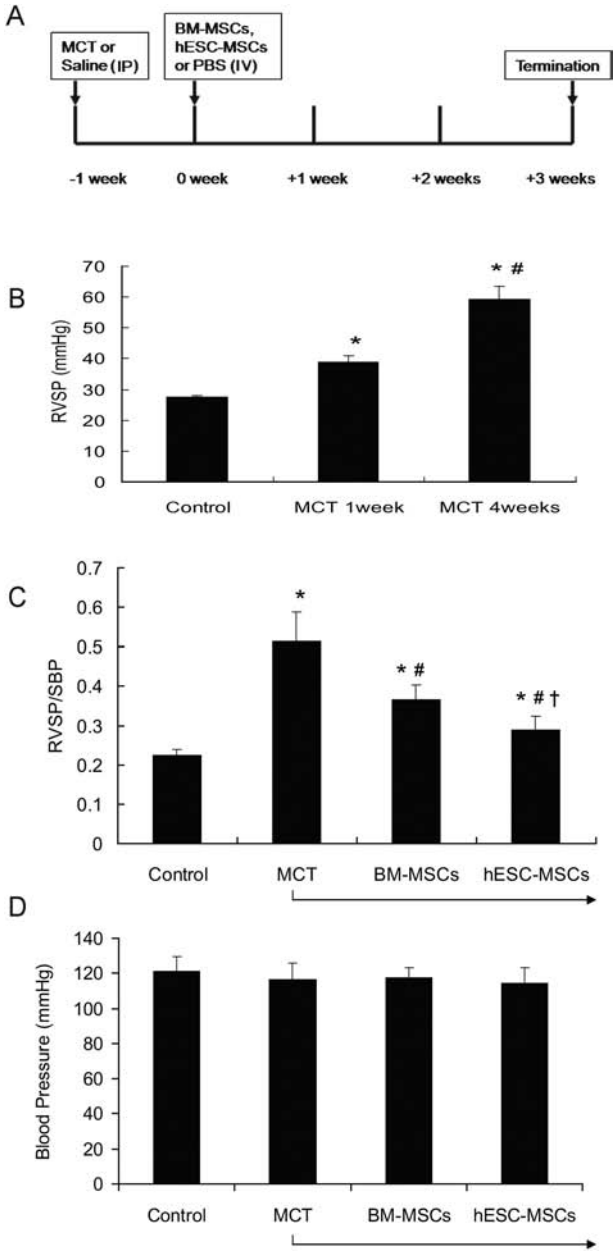

Figure 2. Intravenous transplantation of hESC-MSCs or BM-MSCs attenuated monocrotaline (MCT)-induced pulmonary arterial hypertension (PAH) and right ventricular hypertrophy. (A) Schematic chart shows introduction of PAH and transplantation of hESC-MSCs or BM-MSCs into a PAH mouse model. (B) Right ventricular systolic pressure (RVSP) measured at week 1 and week 4 after MCT administration. The increased RVSP was detected after 1 week of MCT treatment (*$p < 0.01$ vs. control group; #$p < 0.01$ vs. MCT 1 week). (C) RVSP/SBP (systolic blood pressure; relative pulmonary hypertension) ratio was measured at week 4 among mice who received MCT, BM-MSC, or hESC-MSC treatment (*$p < 0.01$ vs. control group; #$p < 0.01$ vs. MCT group; †$p < 0.01$ vs. BM-MSC group). (D) At week 4 after MCT administration, blood pressure (BP) was determined and no major difference was observed among mice who received MCT, BM-MSC, or hESC-MSC treatment.

protective effect of MSC therapy during this early stage of MCT-induced PAH. Therefore, BM-MSCs or hESC-MSCs were injected intravenously 1 week after MCT administration. At 3 weeks posttransplantation (4-week), RVSP was significantly reduced by 27.3% and 45.3%, respectively, in the BM-MSCs and hESC-MSCs groups, compared with MCT group (Fig. 3A, i–ii). Similarly, the ratio of RVSP/SBP was also significantly decreased at 4 weeks in the hESC-MSC group as compared with MCT group (Fig. 2C) ($p<0.01$). Furthermore, RVSP (Fig. 3A) ($p<0.01$) and ratio of RVSP/SBP (Fig. 2C) ($p<0.01$) were also significantly lower in the hESC-MSC group compared with BM-MSC group.

Histological Changes of PAH and MSC Transplantation

As shown in Figure 3B, MCT-induced elevated RVSP was associated with histological evidence of RV hypertrophy. At 4 weeks, the MCT group had a significantly higher RV/(LV + Septum) ratio compared with the control group (Fig. 3B, i–ii) ($p<0.01$). At 3 weeks posttransplantation (4-week), the RV/(LV + septum) ratio was significantly reduced by 15.6% and 26.8% in the BM-MSCs and hESC-MSCs groups, respectively, compared with MCT group (Fig. 3B) ($p<0.01$). This indicates reduced RVSP by BM-MSC or hESC-MSC transplantation attenuated RV hypertrophy in MCT-induced PAH mice. The RV/(LV + septum) ratio was also significantly lower in the hESC-MSC group compared with the BM-MSC group (0.23 ± 0.02 vs. 0.26 ± 0.01; $p<0.01$), suggesting that hESC-MSCs are superior to BM-MSCs in attenuating RV hypertrophy in MCT-induced PAH mice (Fig. 3B).

To examine the potential therapeutic mechanisms of MSCs, we analyzed the anatomic changes in pulmonary arteries at 4 weeks. Morphometric analysis of lung tissues revealed a significant pulmonary vascular remodeling in MCT-treated mice (Fig. 4B). Compared with the control mice (Fig. 4A), MCT-treated mice exhibited

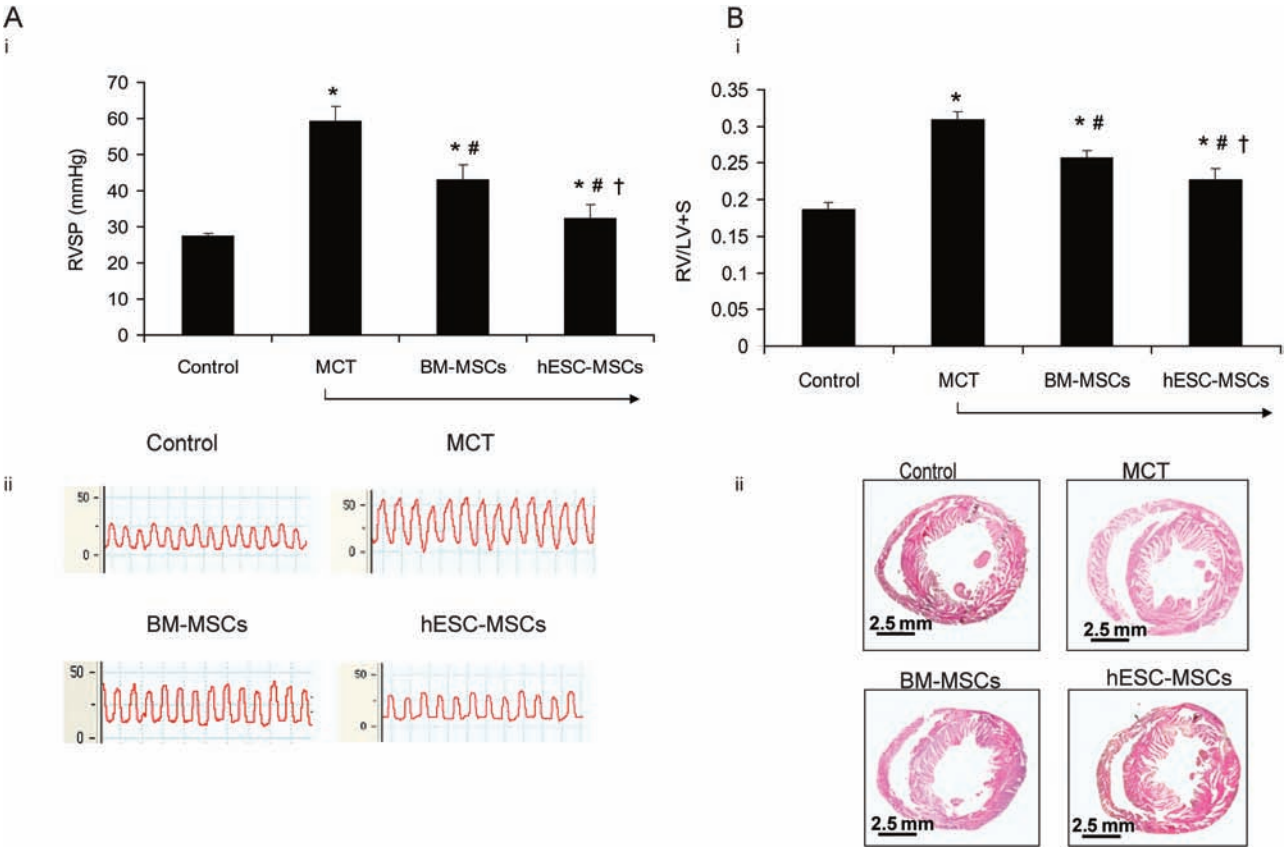

Figure 3. Intravenous transplantation of hESC-MSCs or BM-MSCs attenuated MCT-induced right ventricular hypertrophy. (A) (i) Right ventricular systolic pressure (RVSP) was measured in mice who received different treatments at week 4 following MCT administration (*$p<0.01$ vs. control group; #$p<0.01$ vs. MCT group; †$p<0.01$ vs. BM-MSC group). (ii) Representative photographs show obvious differences in RVSP among mice who received different treatments. (B) (i) The ratio of right ventricular to left ventricular plus ventricular septum (RV/LV + S) weight at week 4 (*$p<0.01$ vs. control group; #$p<0.01$ vs. MCT group; †$p<0.01$ vs. BM-MSCs group). (ii) Representative photographs show right ventricular hypertrophy following exposure to MCT, partially reversed by BM-MSC or hESC-MSC transplantation. Scale bar: 2.5 mm.

significantly greater vessel wall thickness characterized by an excessive muscularization of distal pulmonary vessels and increased vascular stenosis (Fig. 4B, ii–iv). In contrast, BM-MSC or hESC-MSC transplantation significantly attenuated MCT-induced medial wall thickening of the pulmonary arteries (Fig. 4C, D). At 3 weeks after transplantation (4-week), the percentage of medial wall thickness was significantly reduced by 23.9% and 44.1% in the BM-MSC and hESC-MSC groups, respectively, compared with the MCT group (Fig. 4E) ($p<0.01$). The percentage of medial wall thickness was also significantly lower in the hESC-MSC group compared with BM-MSC

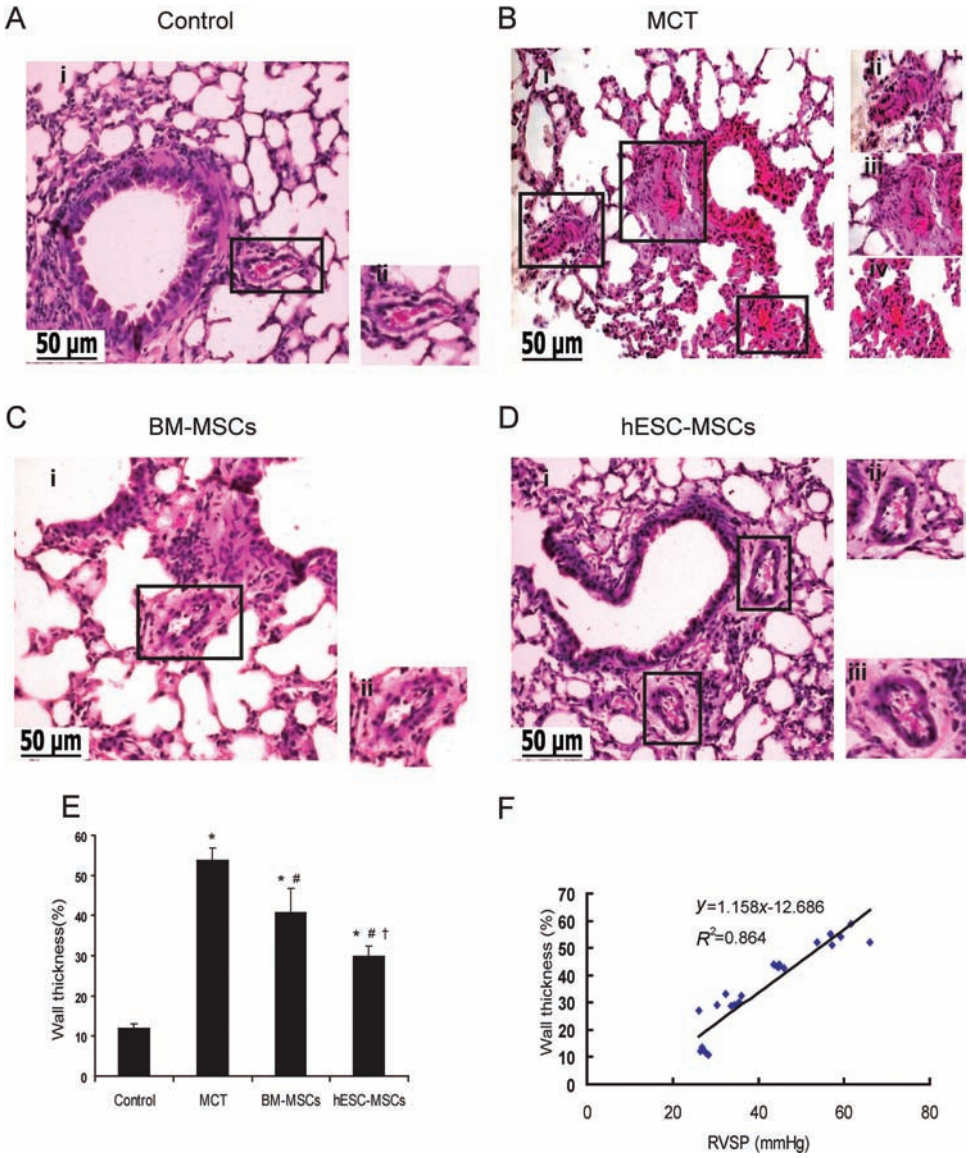

Figure 4. Transplantation of hESC-MSCs or BM-MSCs alleviated MCT-induced pulmonary artery remodeling and enhanced density of pulmonary microvascular beds**.** Through A–D, representative low and high magnification photographs show differential pulmonary vascular changes among mice who received different treatment. (A) (i–ii) Control mice. (B) (i–iv) Mice with MCT treatment displaying complex pulmonary vascular lesions: (ii) Higher-magnification photomicrographs of medial wall thickening. (iii) Lumens of small pulmonary arteries were almost blocked caused by an excessive muscularization. (iv) Severe luminal stenosis with complex vascular lesion. (C) (i–ii) The medial wall thickening in small pulmonary arteries was partially attenuated by BM-MSC transplantation. (D) (i–iii) Medial wall thickening was significantly reduced by hESC-MSC treatment. (E) The percentage medial wall thickness of each artery with an outer diameter ranging between 25 and 100 mm was analyzed. In each mouse, 30 vessels were counted per lung section (*$p<0.01$ vs. control group; #$p<0.01$ vs. MCT group; †$p<0.01$ vs. BM-MSCs group). (F) Relationship between arterial thickness and right ventricular systolic pressure (RVSP). Scale bar: 50 μm.

group (Fig. 4E) (30.1% ± 2.4% vs. 40.9% ± 5.9%; $p < 0.01$). In addition, the percentage of medial wall thickness was significantly and positively associated with elevated RVSP (Fig. 4F) ($r^2 = 0.86$, $p = 0.006$).

Next, we investigated the endothelial protection by MSC transplantation on MCT-induced pulmonary endothelial damage (14). Compared with the control group (Fig. 5A), immunostaining with anti-CD31, an endothelial marker, revealed significantly decreased CD31-positive pulmonary arterial/arteriolar vessels in the lung tissue of MCT-treated mice (Fig. 5B). However, after 3 weeks of transplantation (4-week), the number of CD31-positive arterial/arteriolar vessels had tripled in the BM-MSCs and quintupled in the hESC-MSCs group, respectively, compared with the MCT group (Fig. 5C–E) ($p < 0.01$). Importantly, the number of CD31-positive arterial/

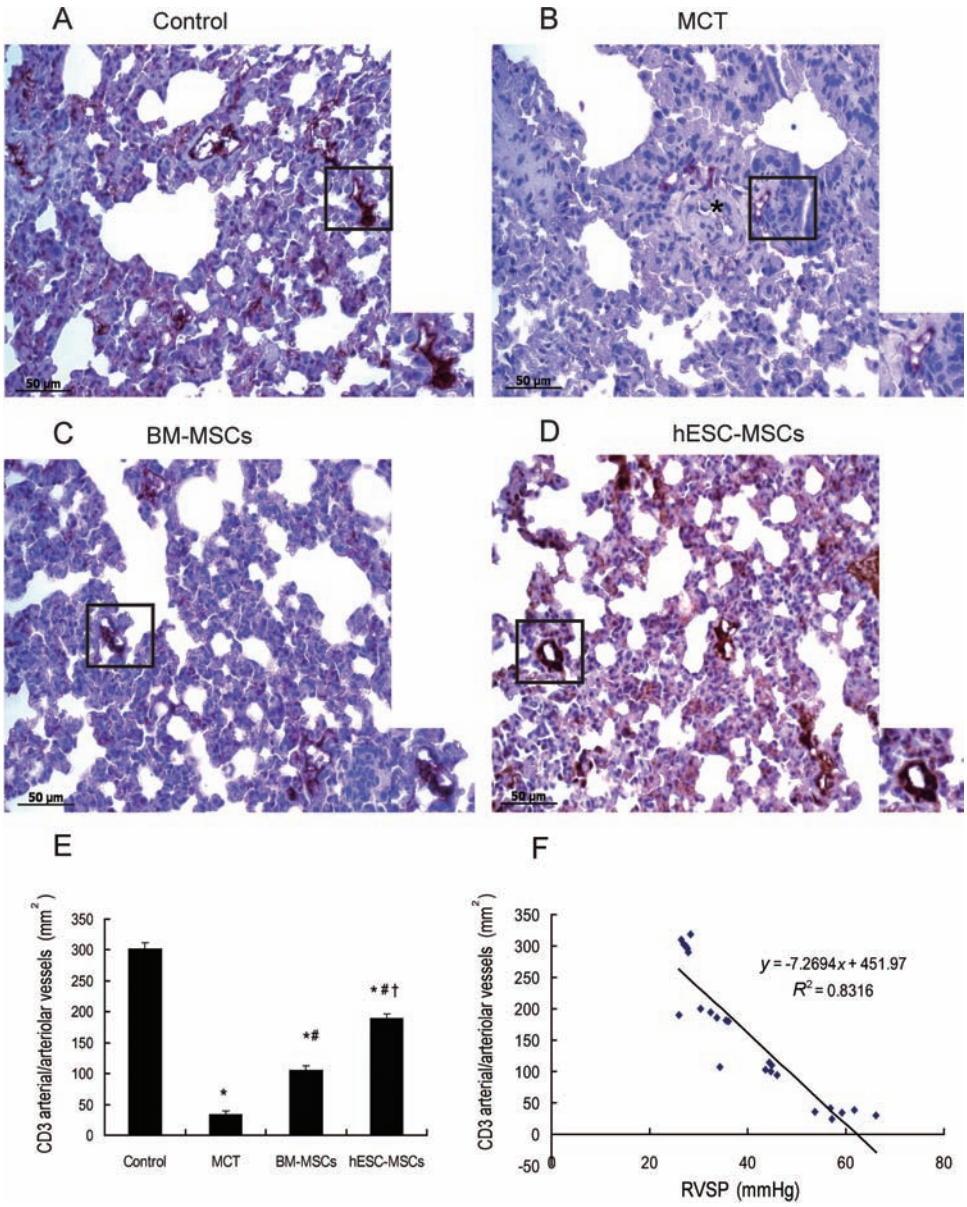

Figure 5. Representative photographs show differential microvascular beds covered by CD31-positive endothelial cells among mice who received different treatment. (A) Control mice. (B) MCT mice (*showing medial wall thickening in a small pulmonary artery). (C) BM-MSC mice. (D) hESC-MSC mice. (E) Quantitative analysis of CD31-positive arterial/arteriolar vessels numbers. Five mice from each group were analyzed, six sections were randomly collected from each mouse and viewed for positive CD31 arterial/arteriolar vessels numbers (*$p < 0.01$ vs. control group; #$p < 0.01$ vs. MCT group; †$p < 0.01$ vs. BM-MSCs group). (F) The association between CD31 arterial/arteriolar vessels density and right ventricular systolic pressure (RVSP). Scale bar: 50 μm.

arteriolar vessels was significantly higher in the hESC-MSCs group compared with BM-MSCs group (Fig. 5E) ($105 \pm 7/mm^2$ vs. $189 \pm 8/mm^2$, $p < 0.01$), indicating hESC-MSCs were superior to BM-MSCs in preventing endothelial damage in MCT-induced PAH mice. Furthermore, the density of CD31-positive arterial/arteriolar vessels was significantly positively associated with elevated RVSP (Fig. 5F) ($r^2 = 0.83$, $p = 0.006$).

Retention and Survival of MSC After Transplantation

The retention and survival ability of hESC-MSCs or BM-MSCs in lung tissue with PAH was examined 1 week (2-week) and 3 weeks (4-week) after transplantation. The transplanted human cells were detected with immunostaining for anti-HNA, PCR for human DNA repeat sequences Alu-sx, and reverse transcription PCR for detection of human-specific growth factors.

One week after transplantation (2-week), immunostaining of lung tissue with anti-HNA revealed both hESC-MSCs (Fig. 6A, i–iii) and BM-MSCs (Fig. 6B, i–iii) were mainly located at pulmonary vessels and nearby extravascular parenchyma. Reverse transcription-PCR analysis revealed gene expression of human vWF as well as human growth factors VEGF and FGF2 in the lung tissue from hESC-MSCs and BM-MSCs groups, but not in the MCT or control group (Fig. 6C). Furthermore, the Bio-Plex cytokine assays demonstrated the presence of human-specific cytokines VEGF, FGF2, and stem cell factor (SCF) in mice lung protein extracts from the hESC-MSC and BM-MSC groups (Fig. 6D). These findings suggest that some transplanted MSCs released cytokines and underwent endothelial differentiation in response to MCT-induced pulmonary vascular injury. Notably, the number of anti-HNA-positive cells retained in the lung tissue 1 week post-transplantation was significantly higher in the hESC-MSC group than the BM-MSC group ($310 \pm 40/mm^2$ vs. $105 \pm 10/mm^2$, $p < 0.01$).

At 3 weeks after transplantation (4-week), the number of anti-HNA-positive cells retained in the lung tissue was significantly decreased in the hESC-MSC group (Fig. 6E) compared with 1 week after transplantation ($310 \pm 40/mm^2$ vs. $45 \pm 8/mm^2$, $p < 0.01$). Interestingly, many of anti-HNA-positive cells observed in the hESC-MSC group were integrated into pulmonary vessels (Fig. 6E, ii) while some were generally distributed in extravascular parenchyma (Fig. 6E). However, at 3 weeks after transplantation, no anti-HNA-positive cells were detected in the BM-MSC group (Fig. 6F). Furthermore, some engrafted hESC-MSCs (Fig. 6G) in small pulmonary vessels were immunoactive for both HNA and endothelial marker CD31, indicating endothelial differentiation of hESC-MSCs in injured lung tissue. Similarly, PCR analysis showed human DNA repeat sequences Alu-sx were detectable only in lung tissue from the hESC-MSC group but not the BM-MSC group (Fig. 6H). In addition, weak expression of human-specific genes FGF2, vWF, and VEGF were detectable in lung tissue from the hESC-MSC group but not the BM-MSC group (Fig. 6I). Indeed, a greater potential of endothelial differentiation in hESC-MSCs (derived from hES-3) was also confirmed by qRT-PCR for human endothelial progenitor marker, Flk-1 (Fig. 1E). These findings indicate that hESC-MSCs are superior to adult BM-MSCs with regard to a long-term survival and differentiation capacity in an injured lung environment.

To closely mimic clinical practice, the transplanted cells were administrated via intravenous injection into wild-type mice after immunosuppression in this study. To exclude the possibility that poor survival of transplanted cells was due to immune rejection, despite the fact that MSCs are thought to possess immune privilege (11), we intravenously delivered the same amount of BM-MSCs into mice with severe combined immunodeficiency. At 1 and 3 weeks of posttransplantation, we observed a significantly decreased number of cell retention (Fig. 6J, i–ii), similar to previous reports (20,42).

Paracrine Effects of MSCs

The differences of paracrine effects between hESC-MSCs and BM-MSCs were investigated. Following exposure of BM-MSCs or hESC-MSCs to serum-free conditioned medium for 48 h, supernatants were collected and screened for 507 human proteins using RayBio® Cytokine Antibody Arrays. Our results demonstrated that both hESC-MSCs and BM-MSCs were able to release a wide spectrum of proteins, including cytokines, chemokines, adipokines, growth factors, angiogenic factors, and soluble receptors. Pair-wise comparison of the protein profiling of hESC-MSC- and BM-MSC-conditioned medium revealed many common characteristics but some distinct differences in paracrine factor profiling. Overall, 398 of 507 factors were commonly detected in both hESC-MSCs and BM-MSCs with <2.0-fold difference. Classification of these factors into bioprocesses disclosed that these secreted factors were involved in metabolism, immunity, and tissue differentiation including vascularization and hematopoiesis. Nonetheless 68 of 507 protein factors were preferentially overpresented in hESC-MSCs (>2.0-fold difference, with the remaining 52 factors preferentially overrepresented in BM-MSCs (>2.0-fold difference).

The top 20 protein factors overrepresented in hESC-MSC-conditioned medium were classified into biological processes using the NIH DAVID Pathway Analysis tool (13) (Table 1). Our results revealed that these protein

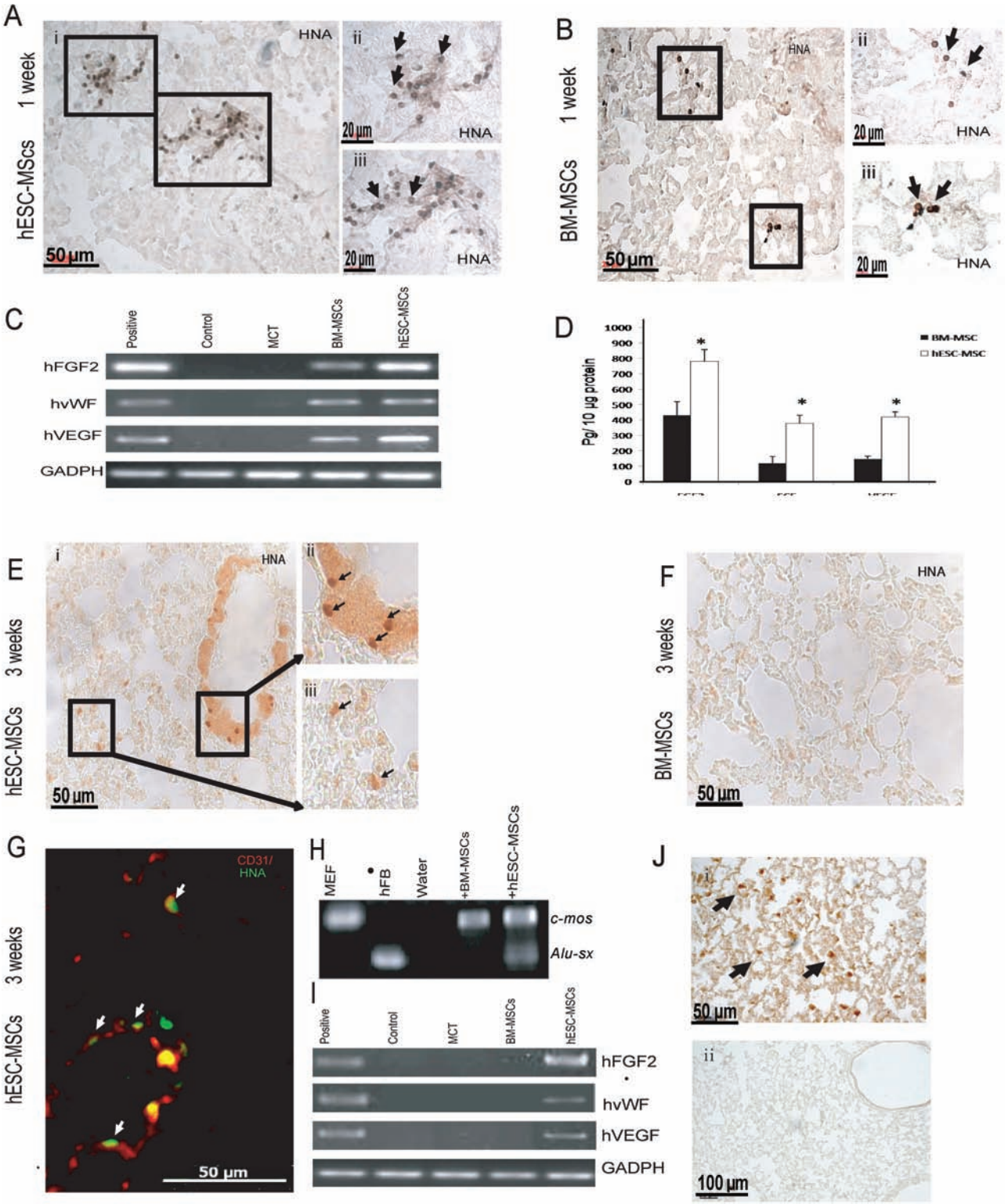
A
1 week
hESC-MSCs
i
HNA
ii
20 μm
HNA
iii
20 μm
HNA
50 μm
B
1 week
BM-MSCs
i
HNA
ii
20 μm
HNA
iii
20 μm
HNA
50 μm
C
Positive
Control
MCT
BM-MSCs
hESC-MSCs
hFGF2
hvWF
hVEGF
GADPH
D
Pg/ 10 μg protein
1000
900
800
700
600
500
400
300
200
100
0
BM-MSC
hESC-MSC
*
*
*
E
3 weeks
hESC-MSCs
i
HNA
ii
iii
50 μm
F
3 weeks
BM-MSCs
HNA
50 μm
G
3 weeks
hESC-MSCs
CD31/
HNA
50 μm
H
MEF
hFB
Water
+BM-MSCs
+hESC-MSCs
c-mos
Alu-sx
I
Positive
Control
MCT
BM-MSCs
hESC-MSCs
hFGF2
hvWF
hVEGF
GADPH
J
50 μm
ii
100 μm

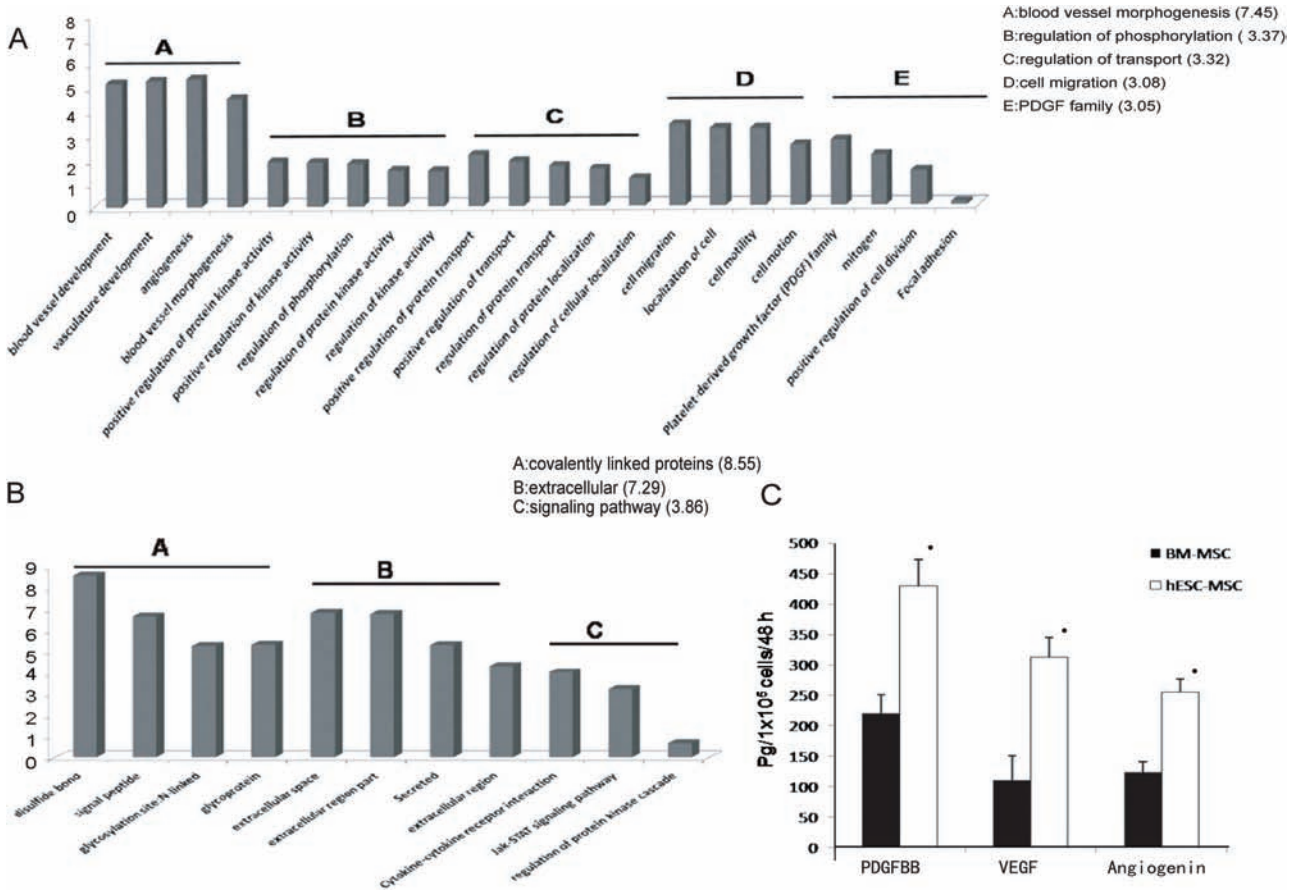

Figure 7. Differential paracrine factor profiling between hESC-MSCs and BM-MSCs secretome. (A, B) Functions and pathways involved in paracrine factor-related genes in hESC-MSCs (A) or BM-MSCs (B) with the NIH DAVID Pathway Analysis tool. Enriched functions and pathways with DAVID cluster score > 3.0 were shown in the figure. The p values were corrected using the Benjamin–Hochberg multiple testing method (5). (C) Quantitative Bio-Plex cytokine assays confirmed human platelet-derived growth factor BB (PDGFBB), VEGF, and angiogenin (ANG) were overpresented in hESC-MSC versus BM-MSC supernatants (*$p < 0.01$ vs. BM-MSCs).

FACING PAGE

Figure 6. Retention and differentiation of hESC-MSCs in response to MCT-induced pulmonary hypertension. (A) At 1 week after cell transplantation, immunostaining of anti-human nuclear antigen (HNA) was detected in hESC-MSC-treated lung tissue (i–iii). High-magnification photographs showing HNA-positive cells were distributed throughout the pulmonary parenchyma and around vessel walls (ii–iii, arrows). (B) Immunostaining of HNA in BM-MSC-treated lung tissue was detected (i–iii). High-magnification photographs demonstrate that HNA-positive cells were distributed throughout the pulmonary parenchyma (ii) and around vessel walls (iii). (C) RT-PCR analysis for human multiple angiogenic and growth factors in lung tissue retrieved 1 week after MSC treatment. It showed expression of fibroblast growth factor 2 (FGF2), von Willebrand Factor (vWF), and vascular endothelial growth factor (VEGF) was detected in hESC-MSC- or BM-MSC-treated mice but was undetectable in those without MSC treatment. (D) Bio-Plex cytokine assays show differential contents of human-specific FGF2, stem cell factor (SCF), and VEGF proteins detectable between BM-MSC- and hESC-MSC-treated lung tissue 1 week after cell transplantation (*$p < 0.05$ vs. BM-MSC group, $n = 3$). (E) At 3 weeks after cell transplantation, HNA-positive cells in hESC-MSC-treated lung tissue were detectable (i–iii). High-magnification photographs show that many of the HNA-positive cells were integrated into pulmonary vessels (ii). (F) At 3 weeks after cell transplantation, HNA-positive cells could not be detected in BM-MSC-treated lung tissue. (G) Some hESC-MSCs were immunoreactive for both anti-HNA and anti-endothelial marker CD31 in small pulmonary vessels (arrows). (H) At 3 weeks after cell transplantation, genomic DNA analysis by PCR for the presence of human *Alu-sx* and mouse *c-mos* repeat sequences between hESC-MSC- and BM-MSC-treated lung tissues. MEF, mouse embryonic fibroblast cells; hFB, human fibroblast cells. (I) RT-PCR analysis from lung tissue retrieved 3 weeks after cell transplantation shows positive expression of human FGF2, vWF, and VEGF in hESC-MSCs but not in BM-MSCs or MCT treated lung tissue. (J) The representative microphotographs showing immunoactivity of HNA in BM-MSC-treated lung tissues retrieved at week 1 (i) and week 3 (ii) after BM-MSC transplantation in SCID mice. Scale bars: 50 μm [A (i), B (i), E (i), F, G, J (i)], 20 μm [A (ii, iii), B (ii, iii)], and 100 μm [J (ii)].

Table 1. Top 20 Proteins Overrepresented in Human Embryonic Stem Cell-Derived Mesenchymal Stem Cells (ESC-MSCs) Versus Bone Marrow-Derived MSCs (BM-MSCs) Detected by Antibody Array

	hESC-MSCs	BM-MSCs	Ratio
EDG-1	289311.35	2541.99	113.81
PDGF-D	10588.81	132.90	79.67
FGF-10/KGF-2	2099.39	42.22	49.73
CCR1	6863.05	157.49	43.58
TWEAK/TNFSF12	4745.06	118.85	39.93
VE-cadherin	20880.95	551.27	37.88
WIF-1	41664.91	1245.51	33.45
EMAP-II	3201.55	98.39	32.54
TIMP-4	8398.55	266.73	31.49
TNF-α	16418.99	601.90	27.28
XEDAR	21299.31	816.58	26.08
VEGF-B	5022.79	194.52	25.82
AR (amphiregulin)	6003.22	292.26	20.54
VEGI/TNFSF15	32015.66	1632.03	19.62
TSLP	5609.80	291.76	19.23
WISP-1/CCN4	15659.29	817.04	19.17
TGF-β RIIb	3534.60	185.37	19.07
SonicHedgehog (ShhNtermial)	5641.95	300.33	18.79
PDGF-C	13830.66	780.76	17.71
Angiogenin	2719.81	156.39	17.39

Table 2. Top 20 Proteins Overrepresented in BM-MSCs Versus hESC-MSCs Detected by Antibody Array

	BM-MSCs	hESC-MSCs	Ratio
HRG-α	7605.38	240.13	31.67
HRG-β1	9581.60	381.50	25.12
LRP-6	1890.50	83.46	22.65
L-selectin (CD62L)	2667.12	121.14	22.02
IL-1 F10/IL-1HY2	6748.74	406.21	16.61
Leptin (OB)	1981.29	130.02	15.24
ICAM-2	3935.04	290.83	13.53
Activin A	21648.15	1615.67	13.40
Insulysin/IDE	1245.79	99.63	12.50
IGF-II R	5506.70	452.24	12.18
IL-21	1564.85	163.71	9.56
Lefty-A	1506.56	182.23	8.27
IL-12 Rβ1	3605.13	447.20	8.06
ICAM-3 (CD50)	2252.91	288.33	7.81
LECT2	1826.05	235.92	7.74
IL-22 BP	2159.10	292.88	7.37
Leptin R	1509.12	212.65	7.10
Luciferase	3904.02	633.30	6.16
Dtk	26062.63	4329.34	6.02
I-309	1717.11	294.06	5.84

factors from hESC-MSCs are associated with early embryonic development, such as embryogenesis, blood vessel morphogenesis, and cell migration (Fig. 7A). Protein factors overrepresented in BM-MSC-conditioned medium (Table 2) are nonetheless associated with late embryonic development, such as extracellular protein synthesis, muscle/skin development and immune response (Fig. 7B).

Selected important human cytokines were quantitatively measured in MSC-conditioned medium using Bio-Plex cytokine assays. Similar to the results of cytokine arrays, human originated angiogenin, platelet-derived growth factor BB, and VEGF were very prevalent in hESC-MSC-conditioned medium compared with those from BM-MSC-conditioned medium (Fig. 7C). These observations demonstrate that the differential profile of paracrine factors from hESC-MSCs and BM-MSCs might account for some of the differences in their therapeutic effect in response to MCT-induced PAH.

DISCUSSION

The results of this study confirm the previous findings (3,37) that MSC transplantation can attenuate elevated RVSP and adverse RV remodeling in an animal model of MCT-induced PAH and provide mechanistic insight into their potential beneficial effects. More importantly, our results at the first time demonstrate that hESC-derived MSCs are superior to adult BM-derived MSCs in attenuation of MCT-induced pulmonary vascular remodeling and endothelial damage. Compared with BM-MSCs, hESC-MSCs derived from early embryonic stages display better survival capacity, more tolerance in an injured lung environment, and wider spectrum of paracrine factors to improve their therapeutic efficacy in attenuation of MCT-induced PAH.

Recent experimental studies have suggested that MSC transplantation is a potential novel therapy for a variety of cardiovascular diseases including myocardial infarction and pulmonary hypertension (11,25,41). In clinical studies (11), adult BM-derived MSCs have been commonly employed, as they are widely available and relatively simple to prepare. Additionally, it has been shown that using MSCs achieves better results than hematopoietic precursors in the treatment of myocardial infarction (2). Although hESC-MSCs and BM-MSCs share many common mesenchymal properties, hESC-MSCs are more proliferative and have a more robust differentiation potential in vivo (21). It has been proposed that MSCs derived from embryonic stage, that is, ESCs, respond better to ischemia with regard to their paracrine potential (23,38,39). This phenomenon is consistent with the observation that MSCs from younger donors or developmentally less mature tissues exhibit more proliferative and differentiation potential and thus resulted in greater therapeutic effects (10). Nevertheless, a comparison of BM-MSCs versus hESC-MSCs in the treatment of cardiovascular disease has not been studied. In this study, we compared the potential therapeutic efficacy of MSCs derived from hESC lines with those derived from adult BM in the treatment of PAH. Compared with BM-MSCs, hESC-MSCs more effectively attenuated MCT-induced occlusive wall thickness of pulmonary arterioles, elevated RVSP, and adverse RV remodeling. Survival of the transplanted stem cells including MSCs remains a critical factor in the success of cell-based therapy (9,20,41). Previous studies have shown a poor long-term retention of MSCs in injured heart (1,28) and lung tissue (33,42) after 3–6 weeks of posttransplantation. Our results showed that hESC-MSCs had better tolerance and higher survival potential than BM-MSCs. Although only a small number of transplanted hESC-MSCs remained detectable in lung tissues at 3 weeks after transplantation, no transplanted BM-MSCs were detected at 3 weeks after transplantation.

Nevertheless, the relatively low rate of cell engraftment and the inefficiency of the transplanted MSCs to differentiate into functional reparative cells in injured tissue do not account for the therapeutic effects of MSC transplantation observed in this study. Prior studies (9,17,31) have suggested that paracine effects rather than de novo vascular regeneration of MSCs may play a more important role in vascular repair and protection. In this study, we observed local expression of human cytokines and growth factors are consistent with the persistence of the transplanted cells. These findings suggest that transplanted MSCs release cytokines in response to MCT-induced injury of the pulmonary vasculature. In addition, using antibody arrays, we demonstrated both similarities as well as differences in the paracrine profiles between hESC-MSCs and BM-MSCs, which might differentially contribute to amelioration of PAH. Analysis of the proteome secretion of hESC-MSCs revealed unique factors that are involved in the biological processes of anti-inflammation, cell survival, proliferation, and differentiation. Some cytokines and growth factors have been shown to be important in cardiovascular protection, such as angiogenin, VEGF, stromal-derived factor (40,45), secreted frizzled related protein (27), interleukin-10 (6), and matrix metalloproteinase-9 (17). These differential paracrine factors released from hESC-MSCs may account for the better survival of the transplanted MSCs and their superior therapeutic efficacy to BM-MSCs for pulmonary vascular protection and repair.

Study Limitations

This study has several limitations. In this study, a mice model of MCT-induced PAH was used rather than the more characterized model in rat. Compared with rat, mice are less susceptible to MCT-induced PAH. Nevertheless, we have tested three different doses of MCT and confirmed the successful creation of PAH in MCT with an optimal dose of 400 mg/kg MCT as reported previously (36). Second, the results of this study may not be applicable to other animal

models of PAH, such as those induced by other toxic agents (e.g., blemycin), molecular stimuli, or hypoxia condition. Indeed, different results have been reported from different animal models of PAH with regard to the therapeutic efficacy of MSC transplantation (32,33). However, none of the currently available animal models can completely recapitulate the entire pathogenesis of PAH in human (8,35). Final MSC transplantation was performed in the early phase of PAH, and the therapeutic efficacy of MSC transplantation in a later phase of PAH remains unclear.

Conclusions

Taken together, our results demonstrate that pluripotent hESC-derived MSCs are superior to adult BM-MSCs in attenuation of MCT-induced PAH in an animal model. Compared to BM-MSCs, a greater potential of hESC-MSCs in PAH treatment may be attributed to a higher capacity of cell survival and more prominent paracrine effects.

ACKNOWLEDGMENTS: This research was supported by HKU Seed Funding for Basic Research (200809159006 to Q. Lian), HKU Small Project Funding (200907176179 to Q. Lian), HKU Strategic Research Theme on Healthy Ageing (to Q. Lian and H.F. Tse), and Collaborative Research Fund of Hong Kong Research Grant Council (HKU 8/CRF/09 to Q. Lian and H.F. Tse). The authors declare no conflicts of interest.

REFERENCES

1. Amsalem, Y.; Mardor, Y.; Feinberg, M. S.; Landa, N.; Miller, L.; Daniels, D.; Ocherashvilli, A.; Holbova, R.; Yosef, O.; Barbash, I. M.; Leor, J. Iron-oxide labeling and outcome of transplanted mesenchymal stem cells in the infarcted myocardium. Circulation 116(11 Suppl):I38–I45; 2007.
2. Arminan, A.; Gandia, C.; Garcia-Verdugo, J. M.; Lledo, E.; Trigueros, C.; Ruiz-Sauri, A.; Minana, M. D.; Solves, P.; Paya, R.; Montero, J. A.; Sepulveda, P. Mesenchymal stem cells provide better results than hematopoietic precursors for the treatment of myocardial infarction. J. Am. Coll. Cardiol. 55(20):2244–2253; 2010.
3. Baber, S. R.; Deng, W.; Master, R. G.; Bunnell, B. A.; Taylor, B. K.; Murthy, S. N.; Hyman, A. L.; Kadowitz, P. J. Intratracheal mesenchymal stem cell administration attenuates monocrotaline-induced pulmonary hypertension and endothelial dysfunction. Am. J. Physiol. Heart Circ. Physiol. 292(2):H1120–H1128; 2007.
4. Barst, R. J.; Gibbs, J. S.; Ghofrani, H. A.; Hoeper, M. M.; McLaughlin, V. V.; Rubin, L. J.; Sitbon, O.; Tapson, V. F.; Galie, N. Updated evidence-based treatment algorithm in pulmonary arterial hypertension. J. Am. Coll. Cardiol. 54(1 Suppl):S78–S84; 2009.
5. Benjamini, Y.; Hochberg, Y. Controlling the false discovery rate: A practical and powerful approach to multiple testing. J. R. Statist. Soc. Ser. B. 57:289–300; 1995.
6. Burchfield, J. S.; Iwasaki, M.; Koyanagi, M.; Urbich, C.; Rosenthal, N.; Zeiher, A. M.; Dimmeler, S. Interleukin-10 from transplanted bone marrow mononuclear cells contributes to cardiac protection after myocardial infarction. Circ. Res. 103(2):203–211; 2008.
7. Crisostomo, P. R.; Wang, M.; Wairiuko, G. M.; Morrell, E. D.; Terrell, A. M.; Seshadri, P.; Nam, U. H.; Meldrum, D. R. High passage number of stem cells adversely affects stem cell activation and myocardial protection. Shock 26(6):575–580; 2006.
8. Dumitrascu, R.; Koebrich, S.; Dony, E.; Weissmann, N.; Savai, R.; Pullamsetti, S. S.; Ghofrani, H. A.; Samidurai, A.; Traupe, H.; Seeger, W.; Grimminger, F.; Schermuly, R. T. Characterization of a murine model of monocrotaline pyrrole-induced acute lung injury. BMC Pulm. Med. 8:25; 2008.
9. Gnecchi, M.; He, H.; Liang, O. D.; Melo, L. G.; Morello, F.; Mu, H.; Noiseux, N.; Zhang, L.; Pratt, R. E.; Ingwall, J. S.; Dzau, V. J. Paracrine action accounts for marked protection of ischemic heart by Akt-modified mesenchymal stem cells. Nat. Med. 11(4):367–368; 2005.
10. Gotherstrom, C.; West, A.; Liden, J.; Uzunel, M.; Lahesmaa, R.; Le Blanc, K. Difference in gene expression between human fetal liver and adult bone marrow mesenchymal stem cells. Haematologica 90(8):1017–1026; 2005.
11. Hare, J. M.; Traverse, J. H.; Henry, T. D.; Dib, N.; Strumpf, R. K.; Schulman, S. P.; Gerstenblith, G.; DeMaria, A. N.; Denktas, A. E.; Gammon, R. S.; Hermiller Jr., J. B.; Reisman, M. A.; Schaer, G. L.; Sherman, W. A randomized, double-blind, placebo-controlled, dose-escalation study of intravenous adult human mesenchymal stem cells (prochymal) after acute myocardial infarction. J. Am. Coll. Cardiol. 54(24):2277–2286; 2009.
12. Heeschen, C.; Lehmann, R.; Honold, J.; Assmus, B.; Aicher, A.; Walter, D. H.; Martin, H.; Zeiher, A. M.; Dimmeler, S. Profoundly reduced neovascularization capacity of bone marrow mononuclear cells derived from patients with chronic ischemic heart disease. Circulation 109(13):1615–1622; 2004.
13. Huang da, W.; Sherman, B. T.; Lempicki, R. A. Systematic and integrative analysis of large gene lists using DAVID bioinformatics resources. Nat. Protoc. 4(1):44–57; 2009.
14. Jasmin, J. F.; Lucas, M.; Cernacek, P.; Dupuis, J. Effectiveness of a nonselective ETA/B and a selective ETA antagonist in rats with monocrotaline-induced pulmonary hypertension. Circulation 103(2):314–318; 2001.
15. Jun, D.; Garat, C.; West, J.; Thorn, N.; Chow, K.; Cleaver, T.; Sullivan, T.; Torchia, E. C.; Childs, C.; Shade, T.; Tadjali, M.; Lara, A.; Nozik-Grayck, E.; Malkoski, S.; Sorrentino, B.; Meyrick, B.; Klemm, D.; Rojas, M.; Wagner Jr., D. H.; Majka, S. M. The pathology of bleomycin-induced fibrosis is associated with loss of resident lung mesenchymal stem cells that regulate effector T-cell proliferation. Stem Cells 29(4):725–735; 2011.
16. Jungebluth, P.; Luedde, M.; Ferrer, E.; Luedde, T.; Vucur, M.; Peinado, V. I.; Go, T.; Schreiber, C.; Richthofen, M. V.; Bader, A.; Haag, J.; Darsow, K. H.; Bartel, S. J.; Lange, H. A.; Furlani, D.; Steinhoff, G.; Macchiarini, P. Mesenchymal stem cells restore lung function by recruiting resident and non-resident proteins. Cell Transplant. 20(10):1561–1574; 2011.
17. Kinnaird, T.; Stabile, E.; Burnett, M. S.; Shou, M.; Lee, C. W.; Barr, S.; Fuchs, S.; Epstein, S. E. Local delivery of marrow-derived stromal cells augments collateral perfusion through paracrine mechanisms (vol 109, pg 1543, 2004). Circulation 112(4):E73–E73; 2005.
18. Lamberts, R. R.; Vaessen, R. J.; Westerhof, N.; Stienen, G. J. Right ventricular hypertrophy causes impairment of left ventricular diastolic function in the rat. Basic Res. Cardiol. 102(1):19–27; 2007.
19. Lang, G.; Klepetko, W. Lung transplantation for end-stage primary pulmonary hypertension. Ann. Transplant. 9(3):25–32; 2004.

20. Li, S. H.; Lai, T. Y.; Sun, Z.; Han, M.; Moriyama, E.; Wilson, B.; Fazel, S.; Weisel, R. D.; Yau, T.; Wu, J. C.; Li, R. K. Tracking cardiac engraftment and distribution of implanted bone marrow cells: Comparing intra-aortic, intravenous, and intramyocardial delivery. J. Thorac. Cardiovasc. Surg. 137(5):1225–1233, e1221; 2009.
21. Lian, Q.; Lye, E.; Suan Yeo, K.; Khia Way Tan, E.; Salto-Tellez, M.; Liu, T. M.; Palanisamy, N.; El Oakley, R. M.; Lee, E. H.; Lim, B.; Lim, S. K. Derivation of clinically compliant MSCs from $CD105^+$, $CD24^-$ differentiated human ESCs. Stem Cells 25(2):425–436; 2007.
22. Lian, Q.; Yeo, K. S.; Que, J.; Tan, E. K.; Yu, F.; Yin, Y.; Salto-Tellez, M.; Menshawe El Oakley, R.; Lim, S. K. Establishing clonal cell lines with endothelial-like potential from CD9(hi), SSEA-$1^{(-)}$ cells in embryonic stem cell-derived embryoid bodies. PLoS One 1:e6; 2006.
23. Lian, Q.; Zhang, Y.; Zhang, J.; Zhang, H. K.; Wu, X.; Lam, F. F.; Kang, S.; Xia, J. C.; Lai, W. H.; Au, K. W.; Chow, Y. Y.; Siu, C. W.; Lee, C. N.; Tse, H. F. Functional mesenchymal stem cells derived from human induced pluripotent stem cells attenuate limb ischemia in mice. Circulation 121(9):1113–1123; 2010.
24. Liang, O. D.; Mitsialis, S. A.; Chang, M. S.; Vergadi, E.; Lee, C.; Aslam, M.; Fernandez-Gonzalez, A.; Liu, X.; Baveja, R.; Kourembanas, S. Mesenchymal stromal cells expressing heme oxygenase-1 reverse pulmonary hypertension. Stem Cells 29(1):99–107; 2011.
25. Mazo, M.; Gavira, J. J.; Abizanda, G.; Moreno, C.; Ecay, M.; Soriano, M.; Aranda, P.; Collantes, M.; Alegria, E.; Merino, J.; Peñuelas, I.; García Verdugo, J. M.; Pelacho, B.; Prósper, F. Transplantation of mesenchymal stem cells exerts a greater long-term effect than bone marrow mononuclear cells in a chronic myocardial infarction model in rat. Cell Transplant. 19(3):313–328;2010
26. Mc Laughlin, V. V.; Mc Goon, M. D. Pulmonary arterial hypertension. Circ. Res. 2006 114(13):1417–1431; 2006.
27. Mirotsou, M.; Zhang, Z. Y.; Deb, A.; Zhang, L. N.; Gnecchi, M.; Noiseux, N.; Mu, H.; Pachori, A.; Dzau, V. Secreted frizzled related protein 2 (Sfrp2) is the key Akt-mesenchymal stem cell-released paracrine factor mediating myocardial survival and repair. Proc. Natl. Acad. Sci. USA 104(5):1643–1648; 2007.
28. Muller-Ehmsen, J.; Krausgrill, B.; Burst, V.; Schenk, K.; Neisen, U. C.; Fries, J. W.; Fleischmann, B. K.; Hescheler, J.; Schwinger, R. H. Effective engraftment but poor mid-term persistence of mononuclear and mesenchymal bone marrow cells in acute and chronic rat myocardial infarction. J. Mol. Cell. Cardiol. 41(5):876–884; 2006.
29. Obata, H.; Sakai, Y.; Ohnishi, S.; Takeshita, S.; Mori, H.; Kodama, M.; Kangawa, K.; Aizawa, Y.; Nagaya, N. Single injection of a sustained-release prostacyclin analog improves pulmonary hypertension in rats. Am. J. Respir. Crit. Care Med. 177(2):195–201; 2008.
30. Osafune, K.; Caron, L.; Borowiak, M.; Martinez, R. J.; Fitz-Gerald, C. S.; Sato, Y.; Cowan, C. A.; Chien, K. R.; Melton, D. A. Marked differences in differentiation propensity among human embryonic stem cell lines. Nat. Biotechnol. 26(3):313–315; 2008.
31. Patel, K. M.; Crisostomo, P.; Lahm, T.; Markel, T.; Herring, C.; Wang, M.; Meldrum, K. K.; Lillemoe, K. D.; Meldrum, D. R. Mesenchymal stem cells attenuate hypoxic pulmonary vasoconstriction by a paracrine mechanism. J. Surg. Res. 143(2):281–285; 2007.
32. Raoul, W.; Wagner-Ballon, O.; Saber, G.; Hulin, A.; Marcos, E.; Giraudier, S.; Vainchenker, W.; Adnot, S.; Eddahibi, S.; Maitre, B. Effects of bone marrow-derived cells on monocrotaline- and hypoxia-induced pulmonary hypertension in mice. Respir. Res. 8:8; 2007.
33. Rochefort, G. Y.; Vaudin, P.; Bonnet, N.; Pages, J. C.; Domenech, J.; Charbord, P.; Eder, V. Influence of hypoxia on the domiciliation of mesenchymal stem cells after infusion into rats: Possibilities of targeting pulmonary artery remodeling via cells therapies? Respir. Res. 6:125; 2005.
34. Roobrouck, V. D.; Ulloa-Montoya, F.; Verfaillie, C. M. Self-renewal and differentiation capacity of young and aged stem cells. Exp. Cell Res. 314(9):1937–1944; 2008.
35. Rosenberg, H. C.; Rabinovitch, M. Endothelial injury and vascular reactivity in monocrotaline pulmonary-hypertension. Am. J. Physiol. 255(6):H1484–H1491; 1988.
36. Song, Y.; Coleman, L.; Shi, J.; Beppu, H.; Sato, K.; Walsh, K.; Loscalzo, J.; Zhang, Y. Y. Inflammation, endothelial injury, and persistent pulmonary hypertension in heterozygous BMPR2-mutant mice. Am. J. Physiol. Heart Circ. Physiol. 295(2):H677–H690; 2008.
37. Spees, J. L.; Whitney, M. J.; Sullivan, D. E.; Lasky, J. A.; Laboy, M.; Ylostalo, J.; Prockop, D. J. Bone marrow progenitor cells contribute to repair and remodeling of the lung and heart in a rat model of progressive pulmonary hypertension. FASEB J. 22(4):1226–1236; 2008.
38. Sze, S. K.; de Kleijn, D. P.; Lai, R. C.; Khia Way Tan, E.; Zhao, H.; Yeo, K. S.; Low, T. Y.; Lian, Q.; Lee, C. N.; Mitchell, W.; El Oakley, R. M.; Lim, S. K. Elucidating the secretion proteome of human embryonic stem cell-derived mesenchymal stem cells. Mol. Cell. Proteomics 6(10):1680–1689; 2007.
39. Timmers, L.; Lim, S. K.; Arslan, F.; Armstrong, J. S.; Hoefer, I. E.; Doevendans, P. A.; Piek, J. J.; El Oakley, R. M.; Choo, A.; Lee, C. N.; Pasterkamp, G.; de Kleijn, D. P. Reduction of myocardial infarct size by human mesenchymal stem cell conditioned medium. Stem Cell Res. 1(2):129–137; 2007.
40. Uemura, R.; Xu, M.; Ahmad, N.; Ashraf, M. Bone marrow stem cells prevent left ventricular remodeling of ischemic heart through paracrine signaling. Circ. Res. 98(11):1414–1421; 2006.
41. Umar, S.; de Visser, Y. P.; Steendijk, P.; Schutte, C. I.; Laghmani el, H.; Wagenaar, G. T.; Bax, W. H.; Mantikou, E.; Pijnappels, D. A.; Atsma, D. E.; Schalij, M. J.; van der Wall, E. E.; van der Laarse, A. Allogenic stem cell therapy improves right ventricular function by improving lung pathology in rats with pulmonary hypertension. Am. J. Physiol. Heart Circ. Physiol. 297(5):H1606–H1616; 2009.
42. van der Bogt, K. E.; Schrepfer, S.; Yu, J.; Sheikh, A. Y.; Hoyt, G.; Govaert, J. A.; Velotta, J. B.; Contag, C. H.; Robbins, R. C.; Wu, J. C. Comparison of transplantation of adipose tissue- and bone marrow-derived mesenchymal stem cells in the infarcted heart. Transplantation 87(5):642–652; 2009.
43. Wagner W, B. S.; Horn, P.; Krunic, D.; Walenda, T.; Diehlmann, A.; Benes, V.; Blake, J.; Huber, F. X.; Eckstein, V.; Boukamp, P.; Ho, A. D. Aging and replicative senescence have related effects on human stem and progenitor cells. PLoS One 4(6):e5846; 2009
44. Xin, Y.; Wang, Y. M.; Zhang, H.; Li, J.; Wang, W.; Wei, Y. J.; Hu, S. S. Aging adversely impacts biological properties of human bone marrow-derived mesenchymal stem cells: Implications for tissue engineering heart valve construction. Artif Organs 34(3):215–222; 2010.
45. Xu, M.; Uemura, R.; Dai, Y.; Wang, Y.; Pasha, Z.; Ashraf, M. In vitro and in vivo effects of bone marrow stem cells on cardiac structure and function. J. Mol. Cell. Cardiol. 42(2):441–448; 2007.